ISSN 1990-7931, Russian Journal of Physical Chemistry B, 2016, Vol. 10, No. 6, pp. 953–962. © Pleiades Publishing, Ltd., 2016.
Original Russian Text © B.P. Aduev, V.A. Anan'ev, A.P. Nikitin, A.A. Zvekov, A.V. Kalenskii, 2016, published in Khimicheskaya Fizika, 2016, Vol. 35, No. 11, pp. 26–36.

COMBUSTION, EXPLOSION, AND SHOCK WAVES

Characteristics of the Initiation of Chain and Thermal Explosions of Energetic Materials by Pulsed Laser Radiation

B. P. Aduev[a, *], V. A. Anan'ev[b], A. P. Nikitin[a], A. A. Zvekov[a], and A. V. Kalenskii[b]

[a] *Institute of Coal Chemistry and Material Science, Siberian Branch, Russian Academy of Sciences, Kemerovo, 650000 Russia*

[b] *Kemerovo State University, Kemerovo, 650000 Russia*

**e-mail: kriger@kemsu.ru*

Received October 14, 2015

Abstract—A comparative experimental and theoretical study of the initiation of silver azide (SA) single crystals and pressed pentaerythritol tetranitrate (PETN)–metal nanoparticles by a neodymium laser pulse is performed. The main differences in the explosive decomposition of the samples are associated with the absence of the induction period and the presence of subthreshold effects in the initiation of PETN-based composites. By contrast, the initiation of SA single crystals always features an induction period, but no subthreshold effects. It is shown that the observed differences in the explosive decomposition are due to the fact that SA single crystals decompose by the chain explosion mechanism, whereas pressed PETN–metal nanoparticles samples, by the thermal explosion mechanism in the micro-hotspot mode. The kinetic parameters of the initiation of the decomposition reaction calculated within the framework of the existing model are consistent with the available experimental data. An experimental criterion for distinguishing between the chain and thermal (in micro-hotspot) mechanisms of the initiation of an explosion under the action of a laser radiation pulse is formulated, according to which the absence of the induction period and a pronounced manifestation of subthreshold effects are indicative of a thermal explosion, whereas the presence of the induction period and the absence of subthreshold effects are characteristic of a chain explosion.

Keywords: solid-state chain reactions, thermal explosion, energetic materials, pulsed laser initiation, PETN, silver azide, nanoparticles, aluminum

DOI: 10.1134/S1990793116060026

INTRODUCTION

Widespread applications of high explosives (HEs) and rising requirements for the safety of their use to motivate the search for new methods to control their reactivity in various conditions [1–3]. Along with experimental work on creating new and studying existing energetic materials, theoretical investigations of reaction mechanisms of initiation of explosive decomposition are of considerable importance. The development of an optical detonator based on silver azide (SA), a primary explosive [4, 5] and secondary HEs [6–10] has been started. For this purpose, the chain explosion model [4, 11, 12] and micro-hotspot thermal explosion model [13–17] were proposed and the energy thresholds of ignition of composite compositions based on a transparent HE containing light-absorbing nanoparticles were experimentally studied [10]. The most important rate constants of the chain reaction were estimated [4, 11, 12, 18–20], and the main features of the initiation of the explosive decomposition of SA single crystals were qualitatively and quantitatively described [4, 11, 20, 21]. The model became the basis for constructing the mechanism of the propagation of explosive decomposition in silver azide crystals [22], the spatial and temporal characteristics of which were experimentally determined in [22, 23].

The micro-hotspot model of the laser initiation of HEs was proposed in [13–17] to interpret the experimentally observed characteristics of the explosive decomposition of pressed lead azide pellets. It was later upgraded to describe the pattern of the laser initiation of secondary explosives containing metal nanoparticles [24–26]. The model takes into account the optical properties of nanoparticles [24, 25] and explains how the nature of the metal [10] and light wavelength [27] influence the critical energy density.

At the same time, despite a significant progress in the development of theoretical concepts, there are no reliable experimental criteria capable of identifying the nature of the explosion, especially that some experimental manifestations of that explosive decomposi-

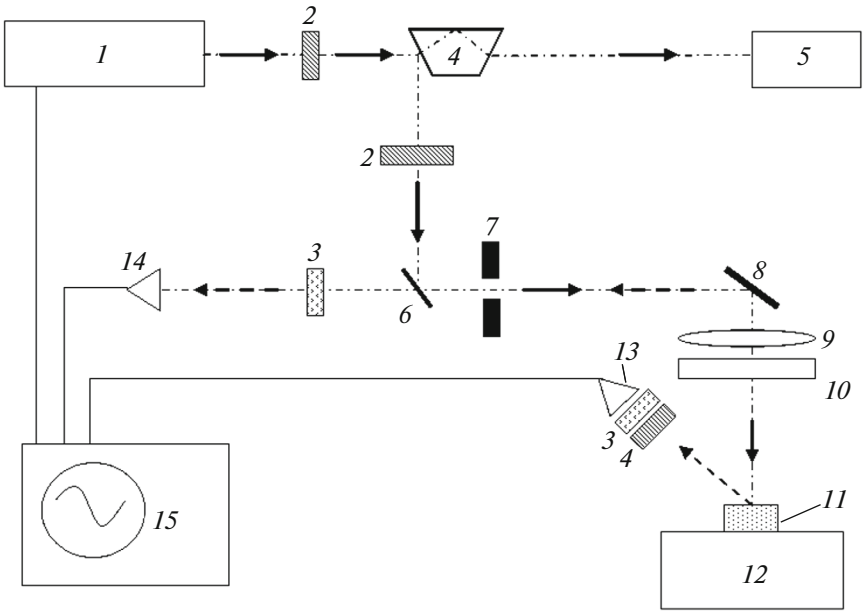

Fig. 1. Schematic diagram of the experimental setup (see the text).

tion can be rather successfully treated in the framework of different model concepts. Today, gaining insights into the mechanism of the explosive decomposition of even a single HE is a complex and time-consuming task, which involves a significant amount of experimental and theoretical work [4, 10–12, 16–27]. Changing the conditions of the experiment, such as the test object (the crystals of different sizes [21] or pressed pellets of various HEs [28–30]), wavelength [17, 31], laser pulse duration [13–15], and laser beam diameter [32, 33], may be accompanied by changes not only in the mechanism, but also in the nature of the initiated explosion.

The aim of the present work was to find relatively easily implementable experimental methods for determining the nature of the explosive decomposition of primary and secondary condensed explosives initiated by a pulsed laser. The task was to perform a comparative experimental study of the kinetics of the luminescence from exploding silver azide (SA) crystals and pressed pentaerythritol tetranitrate (PETN) pellets containing metal nanoparticle in conditions of pulsed laser initiation.

EXPERIMENTAL

The kinetic characteristics of an explosion were studied on a setup the schematic diagram of which is displayed in Fig. 1 and described in detail in [34]. The source of pulsed laser radiation was a Nd:YAG laser *1* operating in the Q-switched mode. The pulse duration at half-height was 14 ns, and the maximum pulse energy at the wavelength of 1064 nm was 1.54 J. The light emission from the explosion was recorded using H6779-01 photomultiplier tubes (PMT) with a temporal resolution of 1 ns. The energy density was varied by using neutral (*2*) and band (*3*) optical filters. The pulse energy was controlled by splitting part of the beam with Dove prism *4* to laser energy meter *5*, which was a IKT-1N calorimeter. A beam with uniform distribution of sample surface irradiance was formed using the projection method [22, 27]. The laser beam passed the optical path shown in Fig. 1 by the solid arrows: interference mirror *6*, forming diaphragm *7* (cut out the middle part of the pulse), rotating mirror *8*, lens *9*, and plate *10* (protected the lens from the expanding explosion products). When sample *11* was a pressed PETN pellet, it was placed on witness plate *12* (aluminum base). For SA crystals (almost transparent at the wavelength of 1064 nm, the first harmonic of the neodymium laser), witness plate *12* was a 0.9-mm-thick glass substrate. The development of the process on the nanosecond time scale was recorded with photomultipliers *13* and *14*. Photomultiplier tube *13*, for panoramic survey, measured the luminescence intensity throughout the experimental cell, whereas PMT *14*, for zone viewing, recorded the time evolution of the emission from the irradiated part of the sample [28, 33]. The signals were fed into digital oscilloscope *15*. The dashed arrows in Fig. 1 show the paths of the emission from the sample recorded by the zonal and panoramic view PMTs.

To control the synchronization of the measured pulse signals and the PMTs, the luminescence produced by irradiating a metal film with a laser pulse was recorded. Upon pulse absorption, the metal vaporized and produced luminescence. While varying the synchronization time and the leading-edge amplitudes of

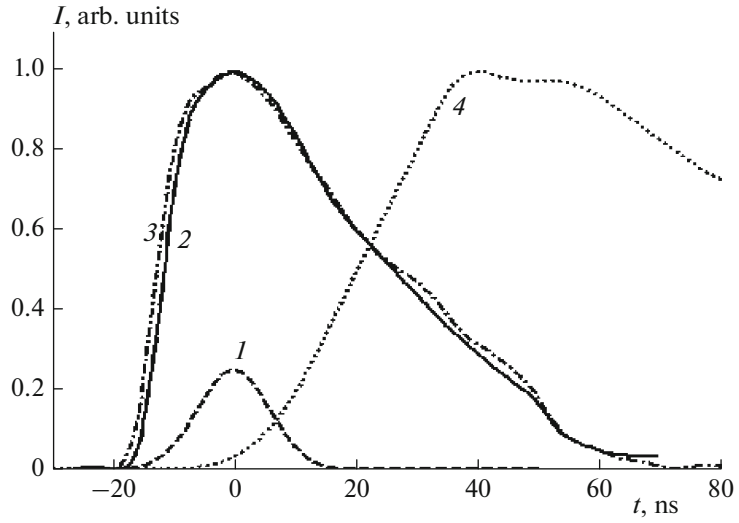

Fig. 2. Time dependence of the intensity of the explosion luminescence from the area of impact of a laser pulse on a pressed PETN–metal nanoparticles pellet: (*1*) initiating pulse, (*2*) PETN–aluminum, (*3*) PETN–cobalt, and (*4*) SA.

the signals, the sum of the squares of the deviations of the PMT signals and the pulse was minimized. Then, the resulting oscillogram was "corrected" for the synchronization time. The measured luminescence intensity signals from exploding pellets were computer processed to determine the induction period and the effective constants of the luminescence signal. The effective rate constant of luminescence rise was calculated by approximating the leading edge of the signal with a Gaussian function.

The test samples were SA crystals with characteristic dimensions of $0.5 \times 0.5 \times 0.4$ mm^3, similar to those used in [4, 17, 31, 33, 35–37]. PETN samples containing 0.1 wt % cobalt and aluminum additives were prepared by mechanically mixing a PETN powder with particle size distribution peak at 1–2 μm, a cobalt powder with a particle radius distribution peak at 100–120 nm, and aluminum powder with a particle diameter distribution peak at 100–110 nm diameter. The sample preparation procedure was described in [9, 10]. As a result pressed pellets, 3 mm in diameter, 1 mm in thickness, (12.2 ± 0.2) mg in weight, and (1.73 ± 0.03) g/cm^3 in density were prepared.

KINETICS OF EXPLOSION LUMINESCENCE

Figure 2 displays a typical experimental dependence of the luminescence from a silver azide crystal initiated by a laser pulse with an energy density of 40 mJ/cm^2. The kinetic dependences of the luminescence intensity (Fig. 2) have a single maximum, with the trailing edge of the pulse being much flatter than the leading. This dependence shows that the luminescence does not appear immediately after the beginning of pulse action: there is a pronounced induction period. In the limit of large excess of the pulse energy density over its critical value (more than fivefold), the induction period duration tends. The latter is defined as the time interval between the peaks of the pulse and luminescence "corrected" for the synchronization time. The experimental dependence of the induction period duration on the pulse energy density normalized by the threshold value for the batch of samples used is shown in Fig. 3. With increasing energy density, the induction period shortens (Fig. 3). In the limit of large excess of the pulse energy density (more than fivefold) over its threshold value, the induction period duration tends to 35 ns. The dependence of the induction period for the explosion of lead azide pressed pellets on the pulse energy density was obtained in [14] using a procedure similar to that described above. As for SA crystals, the induction period duration decreases with increasing laser pulse energy density, but even for a 10-fold excess of the explosion-initiation energy density over the least necessary for initiation, the induction period was reliably determined to be longer than 100 ns.

To investigate the kinetics of the reaction, we carried out a series of measurements at a pulse energy density exceeding the explosion threshold value at least by a factor of two. It was shown [35] that, if the pulse energy density is more than twice the explosion threshold, the initiation of the reaction in the zone irradiated by the laser pulse occurs homogeneously, with the instant of change in the phase state of the material being close to the time at which the luminescence from this zone reaches its maximum. To be quantitatively characterized, the leading edges of the measured luminescence intensity signals were approximated by the error function $I_0(-k^2(t - t_m)^2)$ (Fig. 4). In these coordinates, the dependences are nearly lin-

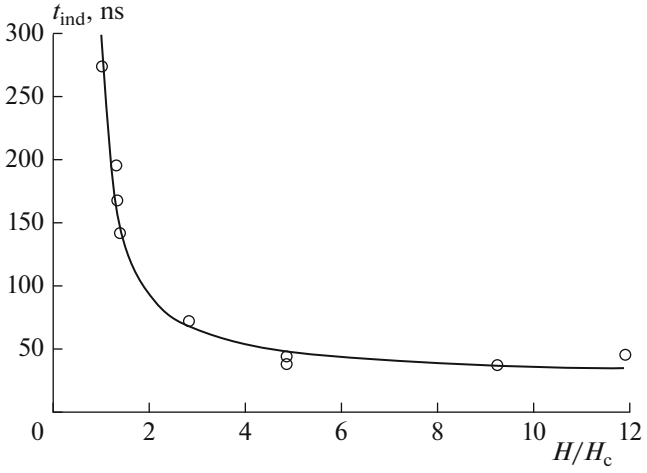

Fig. 3. Measured dependence of the induction period of a SA explosion on the pulse energy density normalized to the threshold value.

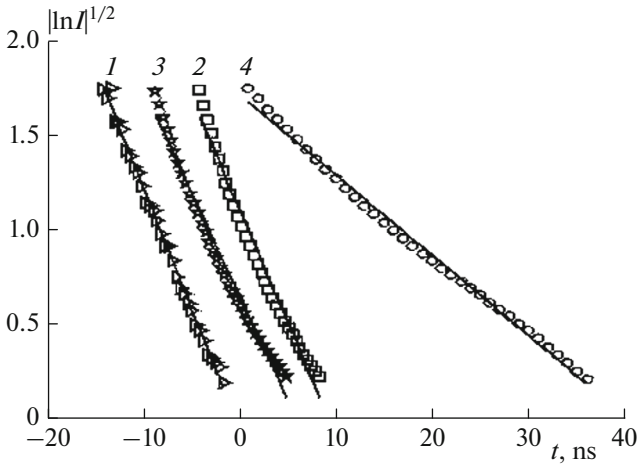

Fig. 4. Time dependences of the explosion luminescence in the error function coordinates: (*1*) initiating pulse; (*2*) PETN–cobalt pellets, subthreshold mode; (*3*) PETN–cobalt pellets, explosion mode; and (*4*) SA, explosion mode. .

ear. The resulting effective constant of luminescence intensity rise was found to be $(4.1 \pm 0.1) \times 10^7$ s^{-1}. This value is much smaller than the effective constant of rise of the pulse, also approximated by the error function: $(1.1 \pm 0.1) \times 10^8$ s^{-1}.

In addition to the kinetic characteristics of the explosive decomposition of traditionally studied HEs, it is necessary to systematize other manifestations of the process, which have been previously disregarded, such as the sound from the explosion, the intensity of the impact on the substrate, and subthreshold effects. The sound from the explosion of SA crystals is weak, like a click. The witness plate exhibits no traces of the impact of the explosion products. The substrate (thin glass) does not crack, only a trace remains from the crystal, which can be easily erased. A glass plate with a surface area of 1 cm^2 can be used to study the kinetic characteristics of 20 explosions, until it begins to crack. At energy densities below the threshold, no luminescence and no any visible changes in the sample were observed. Irradiation of SA crystals repeated up to 10 times caused no increase in the critical energy density, as noted in [25–37]. Covering the SA crystal with a glass plate produces no changes in the critical energy density of explosive decomposition initiation by the first harmonic of a neodymium laser with a beam diameter of more than 100 μm [18, 33].

Irradiation of pressed PETN–cobalt and PETN–aluminum pellets covered with a glass plate caused no explosive decomposition by a pulse with an energy density of less than 1.7 J/cm^2. Figure 5 shows typical luminescence intensity signals from PENT–cobalt and PETN–aluminum pellets in the subthreshold mode (at pulse energy densities insufficient to initiate explosive decomposition), with the PMT signals being shifted by the synchronization time. The kinetic curves feature a single maximum, with the leading edges of the luminescence and pulse profiles coinciding with each other, which means that the luminescence intensity is proportional to the pulse intensity.

Figure 4 shows the leading edges of the time profiles of the luminescence and pulse intensity in the error function coordinates. As can be seen, the pulse profile is closely approximated by this function, which justifies its use in a theoretical analysis. The luminescence intensity signals are described satisfactory; the effective rate constants determined from the slopes of the profiles in these coordinates were used as characteristics of the process.

The effective rate constants of pulse and luminescence intensity rise are similar, $(1.1 \pm 0.1) \times 10^8$ s^{-1}. The characteristic time of luminescence decay was found to be ~40 ns. The total duration of the luminescence was within 100 ns. Although the process in pressed pellets of PETN with nanoparticles of the studied metals occurred in the subthreshold mode sound of an explosion was strong enough, since irradiation causes the cracking of the sample. The beam diameter, 600 μm, is less than the diameter of the pellet, so that, in the area of impact, material is sputtered to form a cavity in the pellet (Fig. 6). For the second-time irradiation of the pellet surface, the energy density needed to initiate explosive decomposition is more than twofold higher.

The kinetic dependences of the luminescence from the explosive decomposition of pressed aluminum nanoparticles–PETN pellets covered with a glass plate caused by a pulse with an energy density of more than 1.7 J/cm^2. One such dependence is shown in Fig. 2. Covering the sample with a glass plate, as in [9, 10], leads to a two- to threefold reduction in the critical energy density for the explosive decomposition of pressed pellets of PETN with aluminum and cobalt

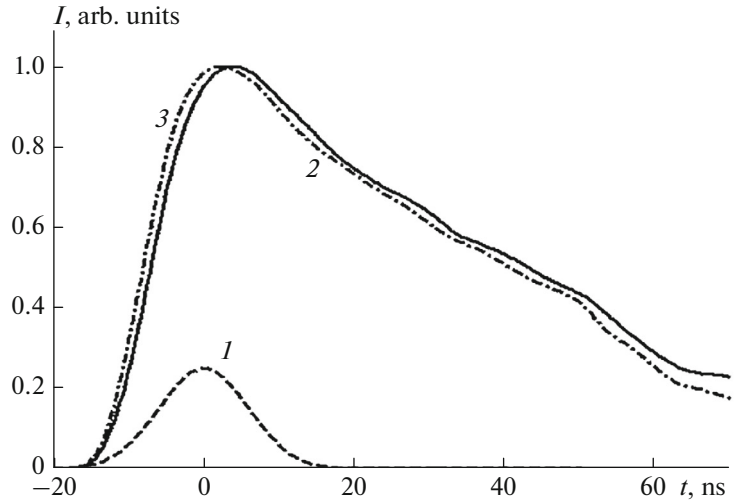

Fig. 5. Time dependence of the intensity of the luminescence from the zone of impact on a laser pulse on a pressed PETN–metal nanoparticles pellet in the subthreshold mode: (*1*) initiating pulse, (*2*) PETN–aluminum, and (*3*) PETN–cobalt.

nanoparticles. The explosion is accompanied by a loud sound and a complete ejection of the explosive material pressed into a copper plate. The explosion of a sample on an aluminum substrate was found to leave a round mark on it. At the the initial stage, the luminescence intensity signal (Fig. 4) is described by a Gaussian function with an effective constant of $k = (1.4 \pm 0.1) \times 10^8\ s^{-1}$. The kinetics of the luminescence intensity from the irradiated area becomes two-peaked, with the first maximum practically coinciding with the maximum of the irradiation intensity, whereas the second being a long plateau with a maximum at ~1800 ns and a decay duration of 2000 ns. A specific feature of the kinetics of the explosives decomposition of pressed PETN–cobalt and PETN–aluminum pellets is the absence of the induction period: the luminescence signal begins simultaneously with the irradiation pulse. In general, the kinetic characteristics of the subthreshold and explosive decomposition of PETN–cobalt and PETN–aluminum pellets are virtually identical.

DISCUSSION OF THE RESULTS

The results of a comparison of the kinetic dependences of the luminescence from the explosion of SA crystals and PETN pellets with metal additives, briefly summarized in the table, are indicative of their qualitative difference. The main similarities are that there is a threshold of initiation of the explosion and that the kinetic dependence can be described by the error function. The principal differences are the absence of the induction period, the existence of pronounced subthreshold phenomena, a reduction in the critical energy density of explosion initiation upon covering PETN-based on compositions with a glass plate.

It is most naturally to attribute the observed differences to distinctions in the mechanisms of explosion initiation in SA crystals and PETN pellets with metal additives. In SA crystals, the reaction is initiated according to the chain explosion mechanism, which postulates an avalanche multiplication of electronic excitations, generated at the expense of the energy released by the decomposition reaction. According to [36], in this case, the light emission of the explosion is associated with intraband luminescence, which can arise due to the generation of electronic charge carriers

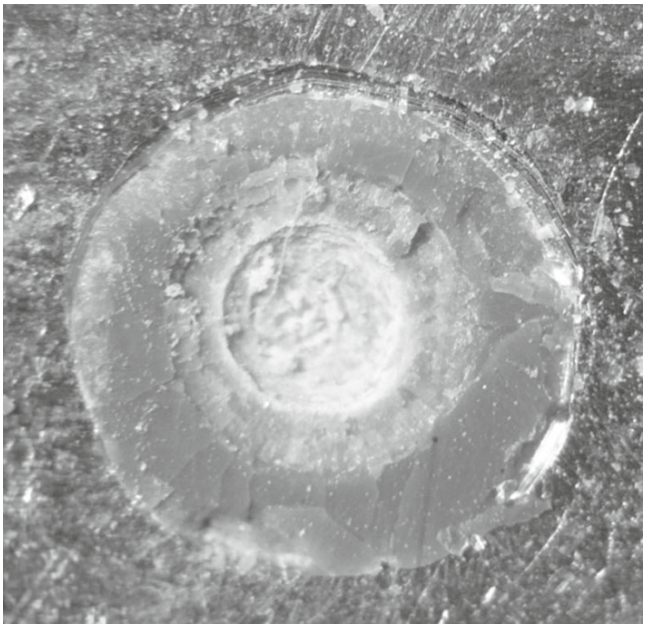

Fig. 6. Photograph of a PETN–aluminum after irradiation with a laser pulse in the subthreshold mode.

Comparison of the characteristics of the pulsed laser initiation of SA crystals and metal nanoparticles–PETN pellets

Samples	Above-threshold explosion	Subthreshold effects	Induction period	Explosion luminescence kinetics
SA crystals	Yes	Absent for sample larger than 50 μm	Decreases with increasing pulse energy density	Leading edge is described by the error function
Pellets				
PETN–cobalt	Yes	Subthreshold luminescence, ejection of material with the formation of a cavity	Absent	″
PETN–aluminum	″	″	″	″

in the depth of the respective band [18]. For light emission to occur, the reaction rate should be high enough so that significant concentrations of chain carriers would accumulate, which gives rise to the induction period observed in studying the kinetics of explosion luminescence. The main source of heating in the chain mechanism of explosion development is the recombination of electron–hole pairs. As a result, the energy released by the reaction dissipates into heat with a significant delay (recombination rate constant is $\sim 10^7$ s^{-1}, which corresponds to 100 ns). Due to this feature, the sample remains "cold" for a considerable time in the course of the development of the decomposition reaction. The temperature rise occurs at the stage of expansion of the explosion products. At an irradiation energy density below the threshold value, no cavity is formed. Covering the sample with a plate does not prevent the expansion of the hot explosion products and does not affect the threshold energy density of explosive decomposition of silver azide crystals irradiated by a first-harmonic pulse of a neodymium laser [17, 31].

Metal nanoparticles–PETN compositions are initiated via the thermal explosion mechanism. The metal nanoparticles in the transparent HE matrix are heated to high temperatures, which leads to the formation of decomposition reaction kernels around them. Achieving significant temperatures in the subthreshold mode leads to the formation of cavities. Rapid heating increases thermoelastic stresses [38, 39] and promotes phase transitions [40] and sample cracking. Covering the sample with a glass plate blocks the escape of material from the irradiated zone, thereby making it possible to initiate the explosion at lower energy densities. Another consequence of high heating temperatures is a rapid onset of emission, before the end of the pulse, even for subthreshold impacts. Above the threshold, the intensity of the emission from the sample increases more rapidly than the laser radiation intensity does (Fig. 2), which indicates the beginning of the reaction and the rapid increase in temperature.

Thus, the observed differences in the kinetic dependences of the luminescence from the explosion of SA crystals and cobalt nanoparticles–PETN pellets make it possible to formulate the criteria that enable to experimentally distinguish the mechanisms of the chain and thermal explosions of condensed explosives by a laser pulse. The characteristic features of a thermal explosion through the formation of microhotspots are the absence of the induction period and the presence of subthreshold effects; by contrast, the chain explosion exhibits a pronounced induction period and no subthreshold effects.

SIMULATION OF CHAIN REACTION KINETICS

In [4, 11], the necessary properties of an energetic solid-state chain reaction:

(1) chain carriers are electronic excitations in the crystal, band electrons, holes, and excitons;

(2) for a pulsed initiation threshold to exist, the order of the reaction of chain carriers recombination must be lower than the order of the branching reaction;

(3) there must be an efficient mechanism of the transfer of energy released in the branching step to the electronic subsystem of the material accompanied by the generation of new electronic excitations.

According to the concept of the deactivation of excited products, the kinetics of the solid-state chain reaction is described by the system of equations

$$\begin{cases} \dot{p} = G - k_r p + 2k_2 p^2 \left(\dfrac{A/2}{A + \gamma_1 p} + \dfrac{A}{A + \gamma_2 p} - 1 \right), \\ \dot{A} = -G + k_r p - 2k_2 p^2 \left(\dfrac{A/2}{A + \gamma_1 p} + \dfrac{A}{A + \gamma_2 p} \right), \end{cases} \quad (1)$$

where p is the concentration of chain carriers, A is the concentration of unexcited sites in the anion sublattice of the sample, G is the rate of the generation of chain carriers, k_r is the rate constant of the recombination of chain carriers constant, k_2 is the rate constant of the bimolecular chain branching reaction, and γ_1 and γ_2 are dimensionless parameters characterizing probability of generating electronic excitations (branching) in

the deactivation of electronically and vibrationally excited nitrogen molecules, respectively. In the first equation of system (1), the chain branching rate is described by the last term, whereas the factor in parentheses is associated with the probability of branching, which is determined by the competition between the different channels of deactivation of excited nitrogen molecules, decomposition reaction products. According to the estimates made in [18, 19], the rate constant for the generation of an electron–hole pair in the deactivation of an electronically excited nitrogen molecule is greater than the rate constant rate of energy transfer to free charge carriers, so $\gamma_1 < 1$. A vibrationally excited molecule is largely deactivated through energy transfer to charge carriers localized at the newly formed site. Since the site is positively charged, the processes of generation of a hole from the ground state and the capture–emission of an electron-emission from the excited level of the defect compete with each other. This competition is characterized by a value of $\gamma_2 \sim 100$.

At small degrees of burnout, model (1) reduces to the model of solid-state chain reaction formulated in [4, 11]. Therefore, model (1) is still capable of describing a number of experimental observations, such as the dependence of the initiation threshold on the pulse duration [11] and microcrystal size [21], the effect of prior irradiation to the critical initiation energy density [5], and the dependence of the induction period of the pulse energy density [11].

Model (1) was used to calculate the kinetic characteristics of the explosion initiation. Since the time evolution of the explosion luminescence intensity is measured in the experiment, the model describing the formation of the luminescence from [36] was used. According to this model, the light emission from a solid sample is due to the intraband luminescence of hot charge carriers formed in the deactivation of excited reaction products. The rate of the generation of hot holes is proportional to the chain branching rate, with the fluorescence intensity normalized by the amplitude being equal to the square of the ratio of the concentration of holes to its maximum value:

$$I/I_m = \left(p/p_m\right)^2.$$

The inverse kinetic problem was solved as follows. First, system of equations (1) was numerically integrated using the Runge–Kutta method of the fifth order with a variable time step and a relative error per integration step not more than 10^{-13}. The generation rate was set in the form $G = G_0 \exp\left(-k_i^2 t^2\right)$, where the effective rate constant of the pulse k_i is related to its duration at half-height τ as $k_i = 2\sqrt{\ln 2}/\tau$. The value of G_0 was set as the product of the critical rate of generation of electron–hole pairs at the current parameters of the model and the degree of exceeding the threshold, which was predetermined for the used batch of samples. Within the interval from 5% of the amplitude of the signal at its leading edge to its maximum (the time of destruction of the sample [35]), the sum of squares of deviations between the experimental and theoretical dependences was calculated, which was minimized using the Nelder–Mead method by varying the recombination rate constant and the dimensionless coefficient γ_2. The bimolecular reaction rate constant was not varied, since the solution of the direct problem showed that its value determines the initiation threshold, while the shape of the kinetic dependences of the reactants at a given degree of exceeding the initiation threshold is virtually independent of its value.

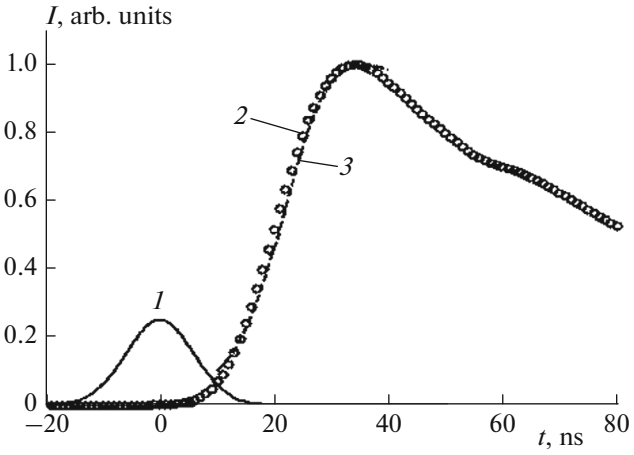

Fig. 7. Time dependences of the explosion luminescence intensity: (*1*) initiating pulse, (*2*) measured time dependence of the explosion luminescence from the impact zone, and (*3*) calculated by model (1).

The result of processing one of the oscillograms is shown in Fig. 7. As can be seen, there is a satisfactory agreement between the predictions of model (1) and the experimental data. The values of the variable parameters obtained by processing 50 explosion luminescence oscillograms was found to be $k_r = (4 \pm 2) \times 10^7\ s^{-1}$, $\gamma_2 = 400 \pm 200$. The value of k_r is consistent with the previous estimates and the values obtained by processing other experimental dependences [4, 11, 21]. Both calculated and measured kinetic dependences exhibit a pronounced induction period (Fig. 7).

KINETICS OF INITIATION OF A THERMAL EXPLOSION

Consider the model of the initiation of a thermal explosion under pulsed heating of a metal nanoparticle located in the bulk of a HE material. The system of differential equations describing the processes of conductive heat transfer in the nanoparticle and in the surrounding HE material, as well as the heat release by the chemical decomposition of the energetic material, reads as [13–16]:

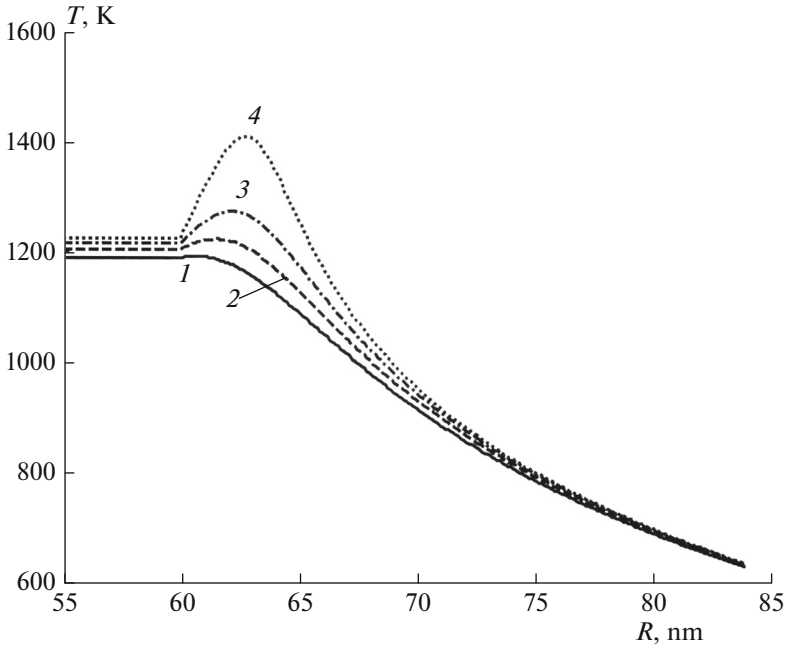

Fig. 8. Spatial distribution of the temperature in the PETN–cobalt system (~60-nm nanoparticles) for its initiation by first-harmonic neodymium laser radiation (1064 nm) at a 10% degree of exceeding the threshold value at various instants of time (in ns): (*1*) 6.0, (*2*) 6.1, (*3*) 6.15, and (*4*) 6.18.

$$\frac{\partial T}{\partial t} = \alpha\left(\frac{\partial^2 T}{\partial x^2} + \frac{2}{x}\frac{\partial T}{\partial x}\right) + k_0\frac{nQ_t}{c}\exp\left(-\frac{E}{k_B T}\right), \quad x > R,$$
$$\frac{\partial n}{\partial t} = -k_0 n\exp\left(-\frac{E}{k_B T}\right), \quad x > R, \quad n_0 = 1, \qquad (2)$$
$$\frac{\partial T}{\partial t} = \alpha_M\left(\frac{\partial^2 T}{\partial x^2} + \frac{2}{x}\frac{\partial T}{\partial x}\right), \quad x < R,$$

where T is the temperature, E is the activation energy of the decomposition process, k_0 is the preexponential factor, Q_t is the heat effect of the reaction, α and α_M are the thermal diffusivities of the matrix and metal nanoparticle materials, c is the volumetric heat capacity of the matrix material, R is the radius of the nanoparticle, n is the relative concentration of HE (PETN), x and t are the current position and time, and k_B is the Boltzmann constant. At the nanoparticle–matrix boundary ($x = R$), laser radiation is absorbed, which leads to the following boundary conditions:

$$\frac{J(t)}{4\pi R^2} - c_M\alpha_M\left.\frac{\partial T}{\partial x}\right|_{x\to R-0} + c\alpha\left.\frac{\partial T}{\partial x}\right|_{x\to R+0} = 0, \qquad (3)$$

where c_M is volumetric heat capacity of the metal and $J(t)$ is the power of absorption of laser pulse radiation. The explosive decomposition of the system under laser heating of the nanoparticles were simulated at the following values of the parameters $\alpha_M = 0.267$ s^{-1}, $c_M =$ 3.74 J/(cm^3 K) (cobalt), $\alpha = 1.1 \times 10^{-3}$ cm^2 s^{-1}, $c =$ 2.22 J/(cm^3 K), $E =$ 165 kJ/(mol K), $k_0 = 1.2 \times 10^{16}$ s^{-1}, and $Q_t =$ 9.64 kJ/cm^3 (PETN) [9, 10, 25–27, 41]. The time profile of the laser pulse radiation power density is close to the normal distribution function Taking as the reference time, the position of the maximum of the pulse intensity, we obtain the following expression for $J(t)$

$$J(t) = \sqrt{\pi}Q_{abs}R^2k_iH\exp\left(-k_i^2t^2\right), \qquad (4)$$

where $k_i = 1.189 \times 10^8$ s^{-1} is the parameter that determines the pulse width (corresponding to the pulse width at half-maximum, 14 ns); Q_{abs} is the absorption efficiency coefficient, which depends on the radius of the nanoparticle; H is the pulsed radiation energy density. At the boundary of the area (nanoparticle and an energetic material layer of thickness $8R$), the first kind boundary condition was set: $T =$ 300 K [41]. The method for calculating the radiation absorption efficiency coefficient Q_{abs} for a spherical inclusion of radius R was described in [10, 25, 27, 42]. The main parameter that determines the $Q_{abs}(R)$ dependence is the complex refractive index m_i, which depends on the nanoparticle material, being, for example, $m_i = 3.7505 - 5.4647i$ [43] for cobalt.

Figure 8 shows a simulation result, within the framework of model (2)–(4), of the process of formation of a kernel of explosive decomposition of energetic material due to the absorption of first-harmonic neodymium laser radiation by a cobalt nanoparticle with $R =$ 60 nm at a 10% degree of exceeding the threshold energy density. The threshold energy density was calculated to be 0.0885 J/cm^2, whereas the absorption efficiency coefficient, calculated within

the framework of the Mie theory for the indicated nanoparticles and a wavelength of 1064 nm, was found to be 0.7642. The time is measured from the point of peak intensity of the laser pulse, as is customary in such problems [13–18, 24–26]. The graph in Fig. 8 shows the formation of an explosive decomposition kernel, which is formed not at the PETN–cobalt boundary, but in the bulk of the energetic material. The time of start of the formation of the reaction kernel is 6 ns, which is comparable with the time it takes for the pulsed radiation intensity to reach 50% of the amplitude at the trailing edge of the pulse. This means that the induction period of the reaction developing by thermal explosion mechanism is virtually nonexistent. As can be seen from Fig. 2, the reaction begins to accelerate rapidly during the pulse just above the critical energy density.

CONCLUSIONS

Thus, a comparative experimental study of the kinetics of the initiation of single crystals of silver azide and pressed metal nanoparticles–PETN pellets by pulsed laser radiation was performed. It was shown that the experimentally observed patterns of the explosive decomposition differ because silver azide single crystals are initiated by the chain explosion mechanism, whereas pressed metal nanoparticles–PETN samples, by the thermal explosion mechanism. The criteria that make it possible to distinguish between the chain and thermal (micro-hotspot mode) mechanisms of the initiation of an explosion by pulsed laser radiation. The latter mechanism is characterized by the virtual absence of the induction period, pronounced manifestations of subthreshold effects (formation of cavities), and the influence of covering the sample surface on the critical energy density. It was shown that the dependence of the time dependence of the luminescence intensity from the explosive decomposition of silver azide is satisfactorily described within a solid-state chain reaction model that takes into account a variety of channels of deactivation of the decomposition products. The experimentally observed short induction period of the explosive decomposition of metal nanoparticles–PETN pellets is closely reproduced in the framework of the micro-hotspot model of a thermal explosion. However, it should be kept in mind that changing the experimental conditions (for example, beam diameter) can change the nature of the explosion.

ACKNOWLEDGMENTS

This work was supported by the Russian Foundation for Basic Research (project no. 14-03-00534 A), grant of the President of the Russian Federation (MK-4331.2015.2), and Ministry of Education and Science of the Russian Federation (research work no. 3603 within the framework of task assignment no. 2014/64).

REFERENCES

1. M. A. Ilyushin, I. V. Shugalei, I. V. Tselinskii, and A. V. Garabadzhiu, Russ. J. Gen. Chem. **83** (13), 2624 (2013).
2. J. Zhang, L. A. Mitchell, D. A. Parrish, and J. M. Shreeve, J. Am. Chem. Soc. **137**, 10532 (2015).
3. A. A. Dippold and T. M. Klapötke, J. Am. Chem. Soc. **135**, 9931 (2013).
4. V. G. Kriger, A. V. Kalenskii, Yu. A. Zakharov, and V. P. Tsipilev, Materialovedenie, No. 9, 14 (2006).
5. N. Fischer, M. Joas, T. M. Klapötke, and J. Stierstorfer, Inorg. Chem. **52**, 13791 (2013).
6. M. A. Ilyushin, I. V. Tselinsky, and I. V. Shugalei, Centr. Eur. J. Energ. Mater. **9**, 293 (2012).
7. J. Evers, I. Gospodinov, M. Joas, T. M. Klapötke, and J. Stierstorfer, Inorg. Chem. **53**, 11749 (2014).
8. M. A. Ilyushin, I. V. Tselinskiy, A. V. Smirnov, and I. V. Shugalei, Centr. Eur. J. Energ. Mater. **9**, 3 (2012).
9. A. V. Kalenskii, M. V. Anan'eva, A. A. Zvekov, and I. Yu. Zykov, Tech. Phys. **60**, 437 (2015).
10. B. P. Aduev, D. R. Nurmukhametov, R. I. Furega, and A. A. Zvekov, Russ. J. Phys. Chem. B **8**, 352 (2014).
11. V. G. Kriger and A. V. Kalenskii, Khim. Fiz., No. 4, 152 (1995).
12. V. G. Kriger, A. V. Kalenskii, A. A. Zvekov, M. V. Anan'eva, and A. P. Borovikova, Russ. J. Phys. Chem. B **3**, 636 (2009).
13. R. S. Burkina, E. Yu. Morozova, and V. P. Tsipilev, Combust. Explos., Shock Waves **47**, 581 (2011).
14. E. I. Aleksandrov and V. P. Tsipilev, Combust. Explos., Shock Waves **20** (6), 609 (1984).
15. E. I. Aleksandrov, O. B. Sidonskii, and V. P. Tsipilev, Combust. Explos., Shock Waves **27** (3), 267 (1991).
16. I. G. Assovskii, *Physics of Combustion and Interior Ballistics* (Nauka, Moscow, 2005) [in Russian].
17. V. M. Lisitsin, V. P. Tsipilev, Zh. Damam, and D. Malis, Combust. Explos., Shock Waves **47**, 591 (2011).
18. V. G. Kriger, A. V. Kalenskii, and A. A. Zvekov, Russ. J. Phys. Chem. B **6**, 15 (2012).
19. A. V. Kalenskii, M. V. Anan'eva, A. P. Borovikova, and A. A. Zvekov, Russ. J. Phys. Chem. B **9**, 163 (2015).
20. A. V. Kalenskii, M. V. Anan'eva, V. G. Kriger, and A. A. Zvekov, Russ. J. Phys. Chem. B **8**, 131 (2014).
21. V. G. Kriger, A. V. Kalenskii, M. V. Anan'eva, and A. P. Borovikova, Combust. Explos., Shock Waves **44**, 190 (2008).
22. V. G. Kriger, A. V. Kalenskii, A. A. Zvekov, M. V. Anan'eva, A. P. Borovikova, and I. Yu. Zykov, Russ. J. Phys. Chem. B **8**, 485 (2014).
23. V. G. Kriger, A. V. Kalenskii, A. A. Zvekov, A. P. Borovikova, and E. A. Grishaeva, Combust. Explos., Shock Waves **48**, 488 (2012).
24. V. G. Kriger, A. V. Kalenskii, A. A. Zvekov, I. Yu. Zykov, and B. P. Aduev, Combust. Explos., Shock Waves **48**, 705 (2012).
25. A. V. Kalenskii, A. A. Zvekov, M. V. Anan'eva, I. Yu. Zykov, V. G. Kriger, and B. P. Aduev, Combust. Explos., Shock Waves **50**, 333 (2014).

26. B. P. Aduev, M. V. Anan'eva, A. A. Zvekov, A. V. Kalenskii, V. G. Kriger, and A. P. Nikitin, Combust. Explos., Shock Waves **50**, 704 (2014).
27. B. P. Aduev, D. R. Nurmukhametov, R. I. Furega, A. A. Zvekov, and A. V. Kalenskii, Russ. J. Phys. Chem. B **7**, 453 (2013).
28. V. I. Korepanov, V. M. Lisitsyn, V. I. Oleshko, and V. P. Tsipilev, Combust. Explos., Shock Waves **42** (1), 94 (2006).
29. Yu. F. Karabanov and V. K. Bobolev, Dokl. Akad. Nauk SSSR **256**, 1152 (1981).
30. E. I. Aleksandrov and V. P. Tsipilev, Fiz. Goreniya Vzryva **18** (2), 100 (1982).
31. V. Lisitsyn, E. Morozova, A. Skripin, and V. Tsipilev, Nucl. Instrum. Methods Phys. Res., Sect. B **286**, 141 (2012).
32. E. I. Aleksandrov and V. P. Tsipilev, Combust. Explos., Shock Waves **17** (5), 550 (1981).
33. V. G. Kriger, V. P. Tsipilev, A. V. Kalenskii, and A. A. Zvekov, Combust. Explos., Shock Waves **45**, 729 (2009).
34. V. P. Tsipilev, Izv. Tomsk. Politekh. Univ. **306** (4), 99 (2003).
35. V. G. Kriger, A. V. Kalenskii, and A. A. Zvekov, Combust. Explos., Shock Waves **46**, 60 (2010).
36. E. D. Aluker, B. P. Aduev, A. G. Krechetov, A. Yu. Mitrofanov, and Yu. A. Zakharov, *Focus on Combustion Research* (Nova Publishers, New York, 2006), p. 55.
37. B. P. Aduev, E. D. Aluker, G. M. Belokurov, A. G. Krechetov, and A. Yu. Mitrofanov, Combust. Explos., Shock Waves **38** (3), 378 (2002).
38. N. N. Nazarenko, A. G. Knyazeva, and Yu. A. Chumakov, Fiz. Khim. Obrab. Mater., No. 6, 50 (2014) [in Russian].
39. S. A. Shanin and A. G. Knyazeva, J. Appl. Mech. Tech. Phys. **55**, 539 (2014).
40. Y. Yang, Z. Sun, S. Wang, and D. Dlott, J. Phys. Chem. B **107**, 4485 (2003).
41. V. G. Kriger, A. V. Kalenskii, A. A. Zvekov, I. Yu. Zykov, and A. P. Nikitin, Thermophys. Aeromech. **20**, 367 (2013).
42. A. V. Kalenskii, A. A. Zvekov, A. P. Nikitin, M. V. Anan'eva, and B. P. Aduev, Opt. Spectrosc. **118**, 978 (2015).
43. A. A. Zvekov, A. V. Kalenskii, B. P. Aduev, and M. V. Anan'eva, J. Appl. Spectrosc. **82**, 213 (2015).

Translated by V. Smirnov